LAND MOVEMENT DETECTION FROM UAV IMAGES

P. C. Pesántez [1, *]

[1] University of Cuenca, Engineering Faculty, Cuenca, Ecuador - (pamela.pesantez)@ucuenca.edu.ec

Commission II, WG II/10

KEY WORDS: Photogrammetry, Land movement, UAV images, Landslide.

ABSTRACT:

In Reina del Cisne (Cuenca-Ecuador) a dynamic sliding process was created due to a cut that was applied at the beginning of the year 2018 to the hillside without technical considerations for the construction of an access road to a house in the sector. From January 2019 to June 2019, period analyzed in this work, the landslide has caused total structural damage (dwellings near the hillside) or partial (houses away from the hillside) and the total collapse of the path that caused the landslide. The field visits and the comparison with CloudCompare of the clouds of points obtained by flights of an unmanned aerial vehicle, UAV between the months of January 2019 and June 2019, have highlighted the high activity of this landslide. The resulting analysis clearly presents the applicability of this technique for early detection of landslides.

1. INTRODUCTION

Landslides are one of the most destructive geological processes affecting humans, causing deaths and property loses, worth tens of trillions of dollars each year (Brabb & Harrod, 1989). In Cuenca-Ecuador, it is a common problem that several of its inhabitants aim to build their homes in steep slopes, due to the low prices of these lands and the accelerated growth of the urban area. These slopes experience landslides, which causes damage to constructions, as is the case of Reina del Cisne sector. It is essential to carry out monitoring of slides which are of vital importance for the mapping of the same, even for the correct urban planning and prevention of the inhabitants at this risk. This monitoring can be carried out by means of classical techniques of topography in situ such as differential GNSS or total station (González-Zúñiga, 2010) combined using active sensors such as RADAR (Bardi et al., 2014; Martire et al., 2016; Ventisette et al., 2014), or Unmanned Aerial Vehicles (UAV) (Dewitte et al., 2008; Martínez-Espejo Zaragoza et al., 2017; Buffi et al., 2017); Satellite images (Behling & Roessner, 2017) among many other alternatives. Detection of large landslides is a major problem and such study requires economic and human resources and long periods of time usually taking weeks or months. In addition, the changing climatic conditions produce morphological variations, due by example to accelerated precipitation. In Ecuador, there are serious problems caused by heavy rains leading to landslides. Therefore, it is necessary to seek solutions to improve the process of detecting areas at risk of mass movements.
The objective of this work is to monitor and record sliding movements located on a steep hillside in Reina del Cisne sector (SE Cuenca) that is affecting a group of homes, conclusions and future work.

2. METHODS

The study area was delimited with PPGIS (Public Participation Geographic Information System). Figure 1 shows the study area. This zone is located at UTM coordinates 17 S area, 726.775 m E and 9.679.327 m N with an elevation of 2.600 m. This area is characterized by steep slopes.

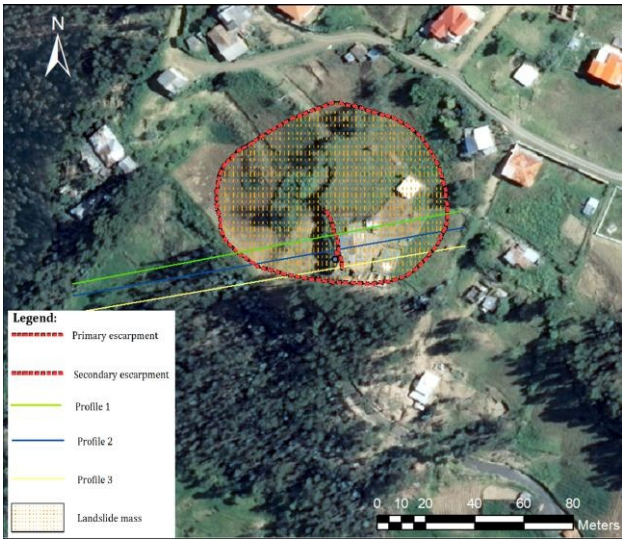

Figure 1. Study area (Cuenca – Ecuador) with information about the landslide and distribution of the profiles studied.

2.1 Generation of point clouds using UAV

The equipment for processing the UAV images was the Drone DJI Phantom 4 RTK®. This equipment is the ideal tool for mapping, inspection, surveying, it has been specifically designed for mapping, it is a compact and easy to fly aircraft with a high-resolution camera, capable of capturing RTK data, with a centimeter level of accuracy and with fewer ground control points compared to traditional tools (Peppa et al., 2019). This UAV allows to obtaining orthomosaics, point clouds and digital elevation model (DEM) with a precision of 3 cm (Mulakala, 2019).

The flight was configured from the Pix4capture© mobile application in double grid flight mode for 3D models (Figure 2).

* Corresponding author

Details	Description
Flight altitude	50 m
Images per flight	219
Flight area	312 x 216 m
Flight time	29 minutes
Ground sample distance	1.45 cm/px

Table 1. Details for January 2019 and June 2019 flights.

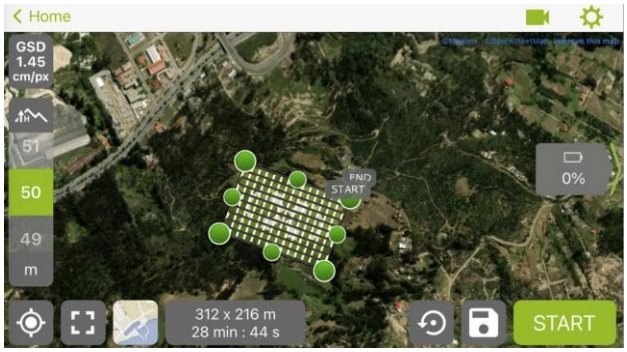

Figure 2. Flight configuration in the Pix4capture© application.

The two sets of images throughout the study area (January 2019 and June 2019), were processed in the Agisoft PhotoScan© software. UAV images processing steps are: 1) photographs selection; 2) camera calibrating; 3) finding homologous points; and 4) identification points over terrain. For this case, the UAV already made corrections in real time, triangulations to adjust the image, generating points clouds, orthophotos and DEM (Núñez Calleja, 2016).

After processing, the 2 point clouds were obtained with a point cloud density as shown in the Table 2.

Date	Points
January 2019	78 million
June 2019	75 million

Table 2. Point clouds density.

2.1.1 Errors obtained in the point clouds generation: The join of scans to form each of the 2 points clouds was satisfactory. Figure 3 shows the highest average error of the 2 dates was only 2.3 cm.

Points	Error (cm)
P1	0.4
P2	2.4
P3	2.7
P4	5.8
P5	2.6
P6	5.2
P7	3.9
Average	2.3

Table 3. Error values in the point clouds generation.

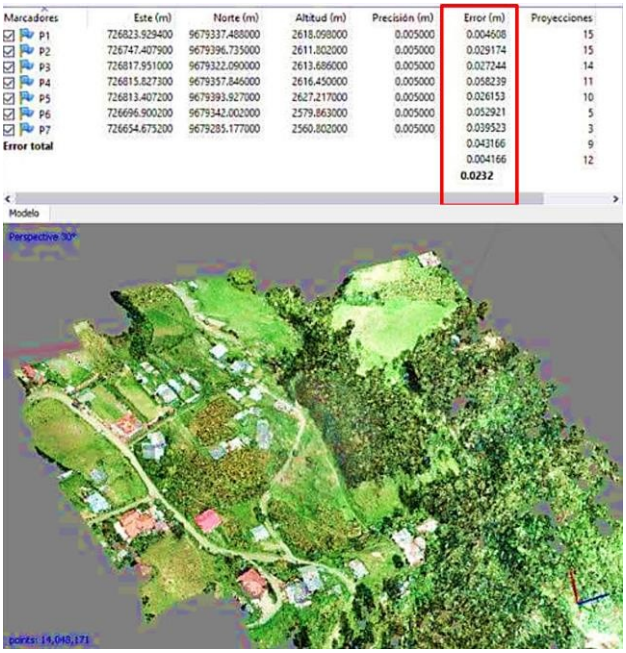

Figure 3. Average errors in m the generation of points clouds.

2.2 CloudCompare

To align and compare in CloudCompare the point clouds of both dates (January 2019 and June 2019) were used 12 static reference points, located outside the landslide area indicated in Figure 4. In addition, a comparison has been made of the deformations that the dwelling has suffered using the same 12 reference points located outside the main escarpment (January 2019 and June 2019).

2.2.1 Errors obtained in the point clouds alignment: The 12 reference points were precisely located and selected in each of the point clouds to align them. The points (A) correspond to the January point cloud and the points (R) correspond to the June point cloud, for the first alignment, which is indicated in Figure 4. The same process was used in the alignment for May 2018 and January 2019 clouds.

The errors achieved in the alignment was low, because all errors have a value less than 1 mm, as shown in Table 4.

Points	Error (mm)
A0 – R0	0.3
A1 – R1	0.2
A2 – R2	0.3
A3 – R3	0.2
A4 – R4	0.3
A5 – R5	0.2
A6 – R6	0.5
A7 – R7	0.3
A8 – R8	0.4
A9 – R9	0.2
A10 – R10	0.3
A11 – R11	0.3

Table 4. Error values in the alignment between January 2019 and June 2019 clouds.

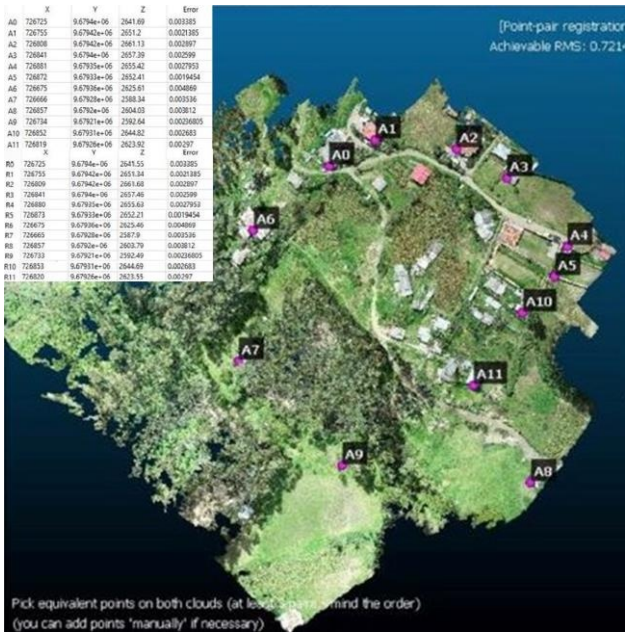

Figure 4. Location of point cloud alignment points with their error values.

2.2.2 Profiling in aligned point clouds: At the end of the alignment of the point clouds (January 2019 and June 2019), 3 profiles are extracted for each point cloud (6 in total) shown in Figure 1 to detect movements caused by the landslide.
Obtaining the profiles is done with the CloudCompare extract cloud section tool as shown in Figure 5, the new point clouds corresponding to the extracted profiles were saved as a LAS file for use in AutoCAD® Civil 3D.

Figure 5. Profile extraction process.

2.2.3 Volume change: Using the aligned point clouds, volume changes were identified between them; taking January 2019 as the reference cloud and June 2019 as the comparison cloud (Figure 6). This process was carried out with Compute 2.5D volume tool.

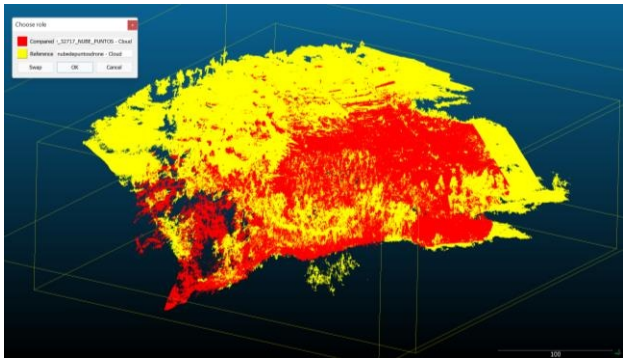

Figure 6. Volume change process, January 2019 (yellow) and June 2019 (red).

2.3 AutoCAD ® Civil 3D

The profiles obtained in CloudCompare are exported to represent, locate and quantify the movements that the landslide has suffered as shown in Figures 7, 9 and 11.

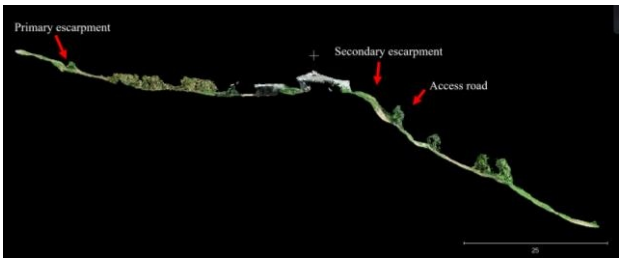

Figure 7. Profile 1 exported to AutoCAD® Civil 3D – Side view.

Figure 8. Profile 1 exported to AutoCAD® Civil 3D – Top view.

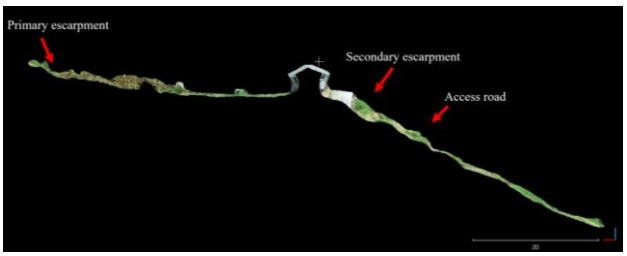

Figure 9. Profile 2 exported to AutoCAD® Civil 3D – Side view.

Figure 10. Profile 2 exported to AutoCAD® Civil 3D – Top view.

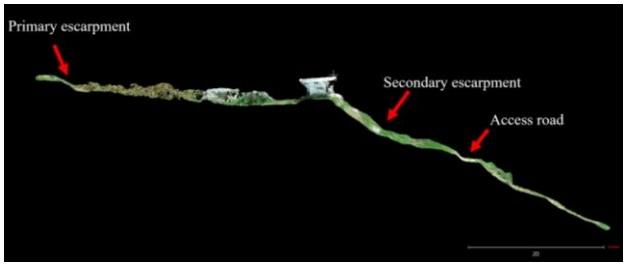

Figure 11. Profile 3 exported to AutoCAD® Civil 3D – Side view.

Figure 12. Profile 3 exported to AutoCAD® Civil 3D – Top view.

3. DETECTION OF LANDSLIDE ACTIVITY BASED ON THE EXTRACTED POINT CLOUDS

The segmentation method for scanning profile was used for comparing profiles, consisting segmenting the point cloud following lines. This technique consists of freely drawing a profile, looking to cross perpendicularly the points. The tracing of this line can be done where it is most convenient (Gonzalez et al., 2004), in this case, it is along the terrain where the landslide has shown more activity and this was observed during the field visits.

Then, the profile representation was generated using AutoCAD® Civil 3D with the profiles extracted from the 2 point clouds (January 2019 and June 2019). This allows obtaining profiles with the respective relevant landslide movements information.

3.1 Procedure with extracted profiles

The method for comparing profiles (January 2019 and June 2019) extracted from CloudCompare consists of 1) export point clouds to AutoCAD® Civil 3D; 2) create a surface from the point cloud; 3) draw a line along the zone of interest at the top of the point cloud; 4) create a profile of the surface to which the line corresponds; 5) extract and display the abscissas and heights information corresponding to the profile. Figures 13, 14 and 15 show the three January 2019 point cloud profiles.

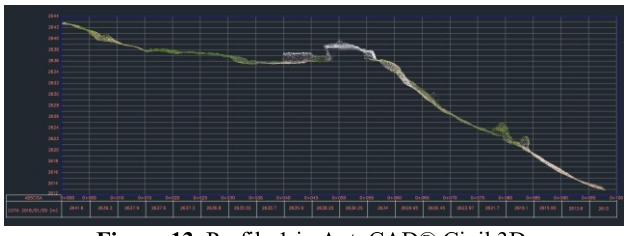

Figure 13. Profile 1 in AutoCAD® Civil 3D.

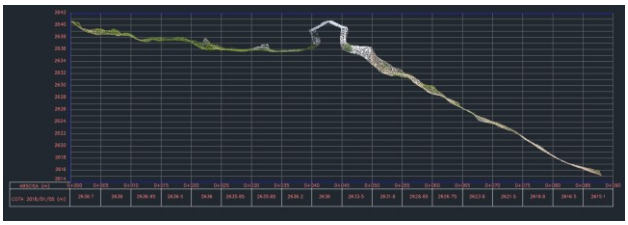

Figure 14. Profile 2 in AutoCAD® Civil 3D.

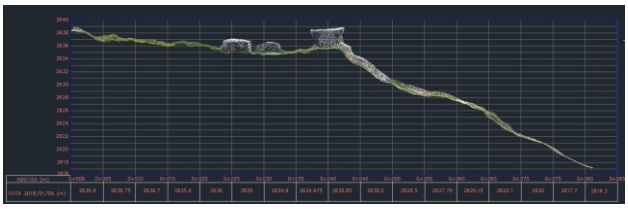

Figure 15. Profile 3 in AutoCAD® Civil 3D.

4. DETECTION OF LANDSLIDE ACTIVITY BASED ON VOLUME CHANGE

The comparison of point clouds using their volume change is a technique that is applied using the Compute 2.5D volume tool; which is convenient for identifying and quantifying volume change efficiently (Štroner et al., 2019).

4.1 Procedure

The method for determining volume change (January 2019 and June 2019) consists of 1) ensure that the point clouds have low alignment errors as indicated in section 2.2.1; 2) select the point clouds of reference (January 2019) and comparison (June 2019); 3) choose an interpolation method for empty cells, in this case the average height method was used; 4) set the characteristics of the volume grid; 5) set the number of steps required to determine the volume change; 6) when identifying volume changes in a landslide, a Z projection should be established. Figure 16 shows the process configuration for this project.

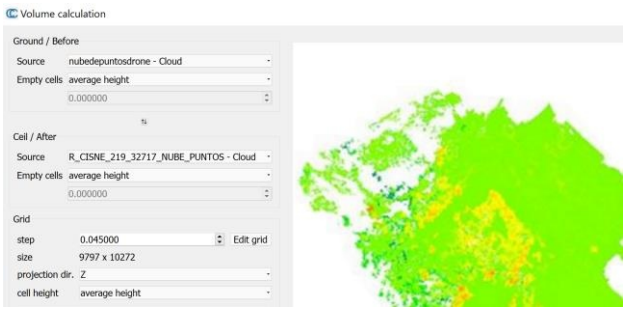

Figure 16. Volume process configuration.

5. RESULTS

For the comparison of profiles, the dimensions of each of the point clouds and their differences were correctly analyzed. For profile comparison, a 5 m division was used for abscissas and a division of 2 m for heights. Each profile has been superimposed both clouds points to illustrate and quantify the deformations that has experienced in the area of study in the period of time analyzed (January 2019 and June 2019).

5.1 Profiles comparison

In Profile 1, 2 and 3, (Figure 1, 17, 18 and 19), it is observed that the growth of corn (abscissa 0+015 to 0+035); in general, it is seen as the ground sinks (abscissa 0+040 to 0+073) and as slowly it is rising (abscissa 0+075 to 0+105).

In Profile 1, (Figure 17) and Profile 3, (Figure 19) are displayed along the same as the recorded terrain movements, although they are removed from the central axis of the landslide these are produced by mini-slides produced by secondary escarpments.

In Profile 2, (Figure 18), it can be noticed that the recorded movements are greater, this is because the profile is located in the central axis of the landslide, besides being influenced by the movements of the mini-landslide produced by a secondary escarpment.

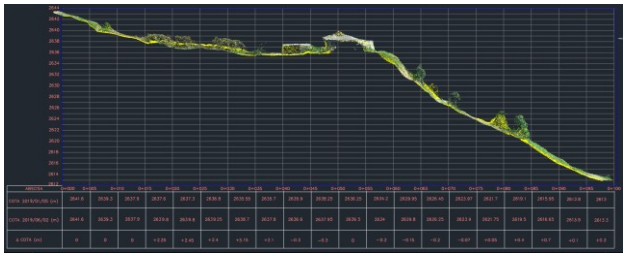

Figure 17. Comparison profile 1, January 2019 (yellow) and June 2019 (RGB).
+: Growth or uplift.
-: Sinking.

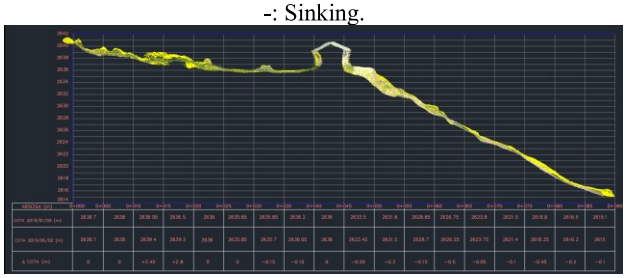

Figure 18. Comparison profile 2, January 2019 (yellow) and June 2019 (RGB).
+: Growth or uplift.
-: Sinking.

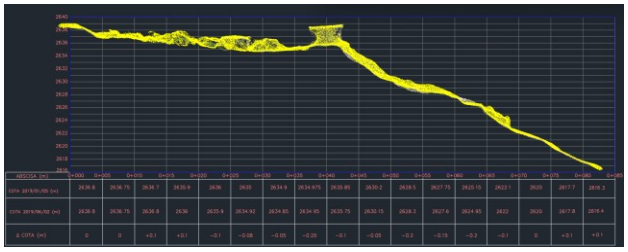

Figure 19. Comparison profile 3, January 2019 (yellow) and June 2019 (RGB).
+: Growth or uplift.
-: Sinking.

5.2 Volume change

It can be seen that in the landslide there were changes in height and volume. No changes are observed in the green areas, because they are outside the landslide.
On the other hand, the landslide area does show changes in height and volume due to the earth movement generated.

In addition, there are some elevations in height due to the growth of trees. In general, a total of 628 cm^3 of material has been removed, which is concentrated in the landslide area.

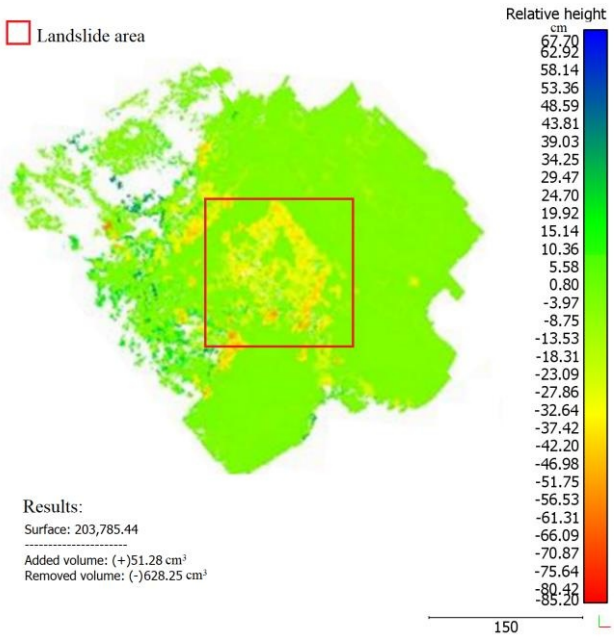

Figure 20. Volume change in the study area.

6. CONCLUSIONS

According to interviews with the residents, the landslide began in the winter of 2015 as a latent, slow slippage that reactivated only in times of heavy rainfall. Cutting into the hillside, transformed this latent and slow slippage into a very active and fast slide.
By virtue of the horseshoe shape of the main scarp of the landslide, its verticality, the absence of deformation in the houses located near the main scarp, the important deformations in the house located in the middle-lower zone of the slid mass, as well as the bulging of the slope in the lower part of the slid mass, it can be concluded that this is a typical rotational landslide.
Additionally, this rotational sliding behavior is verified, since from abscissa 0+015 to 0+085 it is observed that the ground has been sinking; on the contrary to what happens from abscissa 0+085 to 0+105 where the ground begins to rise slightly at a low rate.
In addition, the volume change presented shows that the terrain has lost material due to the landslide.
As well, the use of UAV for this research has been fundamental, since with this technique has been able to reliably detect the movement generated by a landslide; which could help identify areas vulnerable to this type of problem; but UAV technique must be complemented by traditional topography techniques to achieve more accurate results.
It is planned to continue monitoring and structural analysis of buildings in this sector with the fundamental support of aerial images of a drone. In this way, it will be possible to monitor the entire landslide and its surroundings.

ACKNOWLEDGEMENTS

The author wish to thank the Energy Center and the Topography Laboratory of the University of Cuenca for the loan of the terrestrial laser scanner.

REFERENCES

Barbarella, M., & Fiani, M., 2013. Monitoring of large landslides by Terrestrial Laser Scanning techniques: field data collection and processing. European Journal of remote sensing, 46(1), 126-151. doi.org/10.5721/EuJRS20134608.

Bardi, F., Frodella, W., Ciampalini, A., Bianchini, S., Ventisette, C. Del, Gigli, G., … Casagli, N., 2014. Integration between ground based and satellite SAR data in landslide mapping: The San Fratello case study. Geomorphology, 223, 45–60. doi.org/10.1016/j.geomorph.2014.06.025.

Behling, R., & Roessner, S., 2017. Spatiotemporal landslide mapper for large areas using optical satellite time series data. En Workshop on World Landslide Forum (pp. 143-152).

Brabb, E. E., & Harrod, B. L., 1989. Landslides: extent and economic significance. Proceedings of the 28th International Geological Congress: Symposium on Landslides.

Buffi, G., Manciola, P., Grassi, S., Barberini, M., & Gambi, A., 2017. Survey of the Ridracoli Dam: UAV–based photogrammetry and traditional topographic techniques in the inspection of vertical structures. Geomatics, natural hazards and risk, 8(2), 1562-1579. doi.org/10.1080/19475705.2017.1362039.

Eeckhaut, M. Van Den, Poesen, J., Gullentops, F., Vandekerckhove, L., & Hervás, J., 2011. Regional mapping and characterisation of old landslides in hilly regions using LiDAR-based imagery in Southern Flanders. Quaternary Research, 75(3), 721–733. doi.org/10.1016/j.yqres.2011.02.006.

González-Zúñiga, J. C., 2010. Monitorización de deslizamientos de ladera mediante estación total y GPS diferencial. Aplicación al deslizamiento del kilómetro 35+000 de la vía Loja-Cuenca (Ecuador), 71.

Gonzalez, R. C., Woods, R. E., & Eddins, S. L., 2004. Digital image processing using MATLAB. (Vol. 624). PearsonPrentice Hall Upper Saddle River.

Martínez-Espejo Zaragoza, I., Caroti, G., Piemonte, A., Riedel, B., Tengen, D., & Niemeier, W., 2017. Structure from motion (SfM) processing of UAV images and combination with terrestrial laser scanning, applied for a 3D-documentation in a hazardous situation. Geomatics, Natural Hazards and Risk, 8(2), 1492-1504. doi.org/10.1080/19475705.2017.1345796.

Martire, D. Di, Tessitore, S., Brancato, D., Ciminelli, M. G., Costabile, S., Costantini, M., … Calcaterra, D., 2016. Landslide detection integrated system (LaDIS) based on insitu and satellite SAR interferometry measurements. CATENA, 137, 406–421. doi.org/10.1016/j.catena.2015.10.002.

Mulakala, J., 2019. Measurement Accuracy of the DJI Phantom 4 RTK & Photogrammetry. DroneDeploy, Tech. Rep.

Núñez Calleja, P., 2016. Comparativa de software para la realización de ortofotos a partir de imágenes obtenidas por drones.

Peppa, M. V., Hall, J., Goodyear, J., & Mills, J. P., 2019. Photogrammetric assessment and comparison of DJI Phantom 4 pro and phantom 4 RTK small unmanned aircraft systems. ISPRS Geospatial Week 2019.

Revuelto, J., López-Moreno, J. I., Azorín-Molina, C., Arguedas, G., Vicente Serrano, S. M., & Serreta Oliván, A., 2013. Utilización de técnicas de láser escáner terrestre en la monitorización de procesos geomorfológicos dinámicos: el manto de nieve y heleros en áreas de montaña.

Štroner, M., Křemen, T., Braun, J., Urban, R., Blistan, P., & Kovanič, L., 2019. Comparison of 2.5 D Volume Calculation Methods and Software Solutions Using Point Clouds Scanned Before and After Mining. Acta Montanistica Slovaca, 24(4).

Travelletti, J., Malet, J.-P., & Delacourt, C., 2014. Image-based correlation of Laser Scanning point cloud time series for landslide monitoring. International Journal of Applied Earth Observation and Geoinformation, 32(0), 1–18. doi.org/10.1016/j.jag.2014.03.022.

Ventisette, C., Righini, G., Moretti, S., & Casagli, N., 2014. Multitemporal landslides inventory map updating using spaceborne SAR analysis. International Journal of Applied Earth Observation and Geoinformation, 30, 238– 246. doi.org/10.1016/j.jag.2014.02.008.